HHS Public Access

Author manuscript

Sci Transl Med. Author manuscript; available in PMC 2024 May 14.

Published in final edited form as:

Sci Transl Med. 2024 April 24; 16(744): eadj7257. doi:10.1126/scitranslmed.adj7257.

An electroencephalogram microdisplay to visualize neuronal activity on the brain surface

Youngbin Tchoe[1,2,†], **Tianhai Wu**[1,†], **Hoi Sang U**[1], **David M. Roth**[1,3,4], **Dongwoo Kim**[1], **Jihwan Lee**[1], **Daniel R. Cleary**[1,5], **Patricia Pizarro**[1,3], **Karen J. Tonsfeldt**[1,6], **Keundong Lee**[1], **Po Chun Chen**[1], **Andrew M. Bourhis**[1], **Ian Galton**[1], **Brian Coughlin**[7], **Jimmy C. Yang**[8,9], **Angelique C. Paulk**[7], **Eric Halgren**[1,10], **Sydney S. Cash**[6], **Shadi A. Dayeh**[1,11]

[1]Integrated Electronics and Biointerfaces Laboratory, Department of Electrical and Computer Engineering, University of California San Diego, La Jolla, California 92093, United States

[2]Department of Biomedical Engineering, Ulsan National Institute of Science and Technology, Ulsan 44919, Korea

[3]Center for the Future of Surgery, Department of Surgery, University of California San Diego, La Jolla, California 92093, United States

[4]Department of Anesthesiology, University of California San Diego, La Jolla, California 92093, United States

[5]Department of Neurological Surgery, Oregon Health & Science University, Mail code CH8N, 3303 SW Bond Avenue, Portland, Oregon 97239- 3098, United States

[6]Department of Obstetrics, Gynecology, and Reproductive Sciences, Center for Reproductive Science and Medicine, University of California San Diego, La Jolla, California 92093, United States

[7]Center for Neurotechnology and Neurorecovery, Department of Neurology, Massachusetts General Hospital, Boston, MA, USA; Department of Neurology, Harvard Medical School, Boston, MA, USA.

[*]Author to whom correspondence shall be made. S.A.D. sdayeh@eng.ucsd.edu.

[†]These authors contributed equally to this work

Authors contributions: S.A.D., J.C.Y., A.C.P., and S.S.C. conceived the project. S.A.D. led the project. Y.T. and T.W. fabricated the iEEG-Microdisplay, and Y. T. designed the tasks, developed the software, and conducted all data analysis with S.A.D.'s guidance and with input from A.C.P, E.H., and S.S.C. P.C.C. contributed to the fabrication of the GaN μLEDs. H.S.U. performed all surgeries. D.M.R. devised the anesthetic sequence and D.M.R. and P.P. performed anesthesia and mentoring in the pig's operating room. D.K. and A.M.B. contributed to the μLED recording hardware with input from I.G. J.L., D.R.C., and K.L. contributed to the animal experiments. K.J.T. performed histology. The animal experimentation paradigm was developed by Y.T., B.C., J.C.Y., A.C.P., S.S.C., and S.A.D. S.A.D. and Y.T. wrote the manuscript and all authors discussed the results and contributed to the manuscript writing.

Competing Interests: The authors declare the following competing financial interest(s): UC San Diego and MGH have filed a provisional patent application (#63,590,174) on the iEEG-microdisplay titled "Method for Displaying Cortical Activity Directly on the Cortical Surface". Y.T., D.R.C., A.C.P., E.H., S.S.C., and S.A.D. have equity in Cortical Sciences Inc. that is cofounded by the team to commercialize PtNRGrids for intraoperative mapping. S.A.D. was a paid consultant to MaXentric Technologies. D.R.C. and K.J.T. have equity in Surgical Simulations LLC. The MGH Translational Research Center has clinical research support agreements with Neuralink, Paradromics, and Synchron, for which S.S.C. provides consultative input. The other authors declare that they have no competing interests.

Data and materials availability: All data associated with this study are in the paper, supplementary materials or deposited in an open database and can be accessed at DANDI Archive (https://doi.org/10.48324/dandi.000932/0.240317.0101). Custom Matlab code (version R2023a), modified Qt/C++ (version 5.15) open source code for Intan RHD recording controller, and custom Arduino code (version Arduino IDE 2) were used for the analyses and is available in Zenodo (https://doi.org/10.5281/zenodo.10825275).

[8]Department of Neurosurgery, Massachusetts General Hospital, Boston, Massachusetts 02114, United States

[9]Department of Neurological Surgery, Ohio State University, Columbus, Ohio 43210, United States

[10]Department of Radiology, University of California San Diego, La Jolla, California 92093, United States

[11]Department of Neurological Surgery, University of California San Diego, La Jolla, California 92093, United States

Abstract

Functional mapping during brain surgery is applied to define brain areas that control critical functions and cannot be removed. Currently, these procedures rely on verbal interactions between the neurosurgeon and the electrophysiologists. The electrode grids currently used to measure brain activity and to identify the boundaries of pathological versus functional brain regions have low resolution and limited conformity to the brain surface. Here we present the development of an intracranial electroencephalogram (iEEG) microdisplay that consists of free-standing arrays of 2048 GaN light-emitting diodes (μLEDs) laminated on the back of micro-electrocorticography (μECoG) electrode grids. With a series of proof-of-concept experiments in rats and pigs we demonstrate that these iEEG-microdisplays allowed to perform real-time iEEG recordings and display cortical activities by spatially corresponding light patterns on the surface of the brain in the surgical field. Furthermore, iEEG-microdisplays allow to identify and display cortical landmarks and pathological activities from rat and pig models. Using a dual-color iEEG-microdisplay, we demonstrated co-registration of the functional cortical boundaries with one color and displayed the evolution of electrical potentials associated with epileptiform activity with another color. The iEEG-microdisplay holds promise to facilitate monitoring of pathological brain activity in clinical settings.

One Sentence Summary:

An intracranial electroencephalogram microdisplay to monitor brain activity in real-time on the surface of the brain in the surgical field.

INTRODUCTION

The goal of neurosurgical treatment is complete resection of pathologic tissue. However, there is usually a trade-off between the extent of resection and the risk of postoperative neurological deficit due to loss of functional tissue (1-6). Because brain lesions can distort normal anatomy and cause functional reorganization (7) that may not be fully identified with non-invasive functional neuroimaging techniques, direct electrical stimulation (DES) paired with electrophysiological recording has evolved as the gold standard for determining functional boundaries before resection of lesions located in eloquent areas (8-12). DES is a reliable, safe, and effective technique for the identification and preservation of cortical and subcortical neuronal pathways for motor, sensory, language, and memory function(8, 12). More recently, passive electrophysiological recordings in the high gamma band (60-200

Hz) were shown to be a fast, robust, and reliable method for identifying receptive language areas (13) with differences in brain activity entropy and high gamma activity characterizing pathological tissue in brain tumors(3, 14, 15). Based on DES mapping, functional regions are marked and preserved from resection, usually with a margin of about 5 mm around the motor areas and 7 mm around the language areas to avoid post-operative functional deficit(16). Most commonly, identifying the spatial extent of functional and pathological boundaries based on neurophysiology is communicated verbally by messages written on paper that is transported across the operating room between the intraoperative monitoring team comprised of clinical electrophysiologists and neurologists and the neurosurgeons. Moreover, some groups use sterile paper placed on the surface of the brain to mark areas for resection and areas for preservation (17, 18). Clearly, the resolution and the methodology for presenting this critical information to guide neurosurgical interventions can be improved.

Recent advances in thin-film microelectrode technology have increased the resolution by which cortical activity can be measured and localized (19-21). For example, platinum nanorod grids (PtNRGrids) have been used to identify the curvilinear boundary between functional and pathological tissues in the human brain at unprecedented spatial resolution(21). However, to date, there is no available technology that can display these cortical boundaries in situ on the brain. The rise of flexible panel display technology presents an opportunity to revolutionize the way we measure and display cortical activity. In the display technology field, gallium nitride (GaN) light emitting diodes (LEDs) represent an efficient and scalable solution for solid-state lighting and displays(22), and have recently progressed to full-color capability with layer-transfer techniques of micro-LEDs (μLEDs) (23). However, the monolithic integration, encapsulation, and release of free-standing GaN μLED arrays from wafers suitable for production scale with diameters exceeding 6” has not been previously accomplished.

To address the need for high fidelity, real-time tracking of functional and pathological brain activity as well as advance the use of GaN μLED display tools, here we describe a fabrication procedure for flexible GaN μLEDs and the application of this innovation to a flexible brain electroencephalogram micro-display (iEEG-microdisplay). The iEEG-microdisplay comprises GaN μLEDs mounted behind the PtNRGrids, as well as acquisition and control electronics and software drivers to analyze and project the cortical activity directly from the surface of the brain. We demonstrated the safe and effective use of the iEEG-microdisplay through benchtop characterization. Moreover, we demonstrated highly localized brain activity could be projected through the light display in the iEEG-microdisplay in experiments in rats and pigs. In the pig model, we demonstrate that the iEEG-microdisplay provided automated and real-time visual representation of somatosensory evoked potentials (SSEPs). In addition, large voltage deflections correlated with epileptic discharges were co-registered to mapped sensory regions using a dual-color iEEG-microdisplay. In the rat model, we show that the iEEG-microdisplay resolved and represented individual cortical columns and displayed pathological activity with high definition. The combination of PrNRGrids, which allow detection of fine resection boundaries in human brains (21), with iEEG-microdisplays which display cortical activities with spatially corresponding light patterns might help to advance neurosurgical procedures.

RESULTS

iEEG-microdisplay development

To construct the iEEG-microdisplay, we combined ultrathin PtNRGrids previously used for μECoG (21), with GaN μLEDs. We chose GaN μLEDs over soft organic LEDs because they are highly efficient and consume low power (23, 24) thereby producing low thermal heating losses and inducing minimal heating effects on the cortical tissue(25). Additionally, the high intensity of light produced by GaN μLEDs is visible to the human eye even under the bright surgical lightning(26). To fabricate flexible GaN μLED arrays for both high resolution and broad spatial coverage, we developed a scalable process on 6-inch GaN/polycrystalline AlN engineered engineered Qromis® Substrate Technology™ (QST) substrate(27, 28) and released ultrathin μLED arrays, some with 1024 and some with 2048 pixels, embedded in polyimide layers (see fig. S1). GaN μLEDs with indium gallium nitride (InGaN) quantum wells emitting blue light with peak wavelength of 450 nm (fig. S2). In order to simultaneously display and co-register normal and diseased cortical activity, we used ink-jet printing to deposit quantum dot color conversion (QDCC) inks made of indium phosphide (InP) quantum dots on the surface of the GaN μLEDs (fig. S2)(29). This allowed us to emit multiple colors, enabling richer and more nuanced visual representation of neural activity patterns. The flexible GaN μLED arrays were then laminated on the back of the PtNRGrids grids (Fig. 1A)(21) to form the iEEG-microdisplay. The PtNRGrids were constructed on thin and brain-conformal parylene C substrates with thousands of channels which reliably recorded the spatiotemporal dynamics of brain activity at high-resolution and with broad coverage (21, 30). As both the flexible μLED array and μECoG were based on scalable, and reconfigurable manufacturing processes, we matched their pitch and coverage for a single iEEG-microdisplay. Here, we discuss results based on displays with 32mm × 32mm coverage and 1mm pitch used for pig brains (Fig. 1A), and 5mm × 5mm coverage with 0.15mm pitch for rat brains (Fig. 1B). The single-color iEEG-microdisplay was composed of 1024 PtNR recording contacts and 1024 GaN μLED pixels. The dual color iEEG-microdisplay comprised 2048 QDCC-printed GaN μLEDs with 0.4mm vertical and 0.5mm horizontal pitches, and a corresponding PtNRGrid with 1024 contacts with 0.8mm vertical and 0.5mm horizontal pitches, both providing a 12.8mm × 32mm brain coverage (fig. S2, C and D). The μECoG grids utilized 30 μm diameter PtNR contacts with an average impedance of 30kΩ at 1kHz. The size of an individual GaN μLED varied depending on their intended use. Specifically, GaN μLEDs with a diameter of 220μm were optimized for 1 mm pitch iEEG-microdisplay (Fig. 1A), whereas those with a diameter of 100μm were designed for iEEG-microdisplays with higher densities such as that used for the rat (Fig. 1B) or dual-color 2048 μLEDs used for the pig (fig. S2, C and D).

Part of the electrical input supplied to LEDs is not converted to light but lost as thermal energy. The consequential increase of the cortical surface temperature must be kept below 1°C (31, 32). To ensure that this is the case for our iEEG-microdisplay, we have characterized the thermal and electrical safety of the iEEG-microdisplay. In one experiment, we turned on all 2048 μLEDs at their maximum brightness possible with our LED driver chip as the iEEG-microdisplay was placed on top of the pig's brain for 30 minutes. The temperature was then monitored with an infrared (IR) imaging camera. No temperature

changes within the measurement resolution of the IR camera (0.1 °C) were observed (Fig. 1C). Additionally, post-mortem histochemical analysis of the same pig's brain showed undetectable differences in the structure of the cortical surface under the iEEG-microdisplay and the contralateral region (fig. S3): The top cortical layer was of comparable thickness, the neuronal density was similar, and the neuron shape was normal. However, when the same experiment was conducted on a rat's brain with the high-density iEEG-microdisplay whose pixel pitch was 0.15mm, we observed a temperature increase of up to 6°C in less than 5 minutes when all 1,024 μLEDs were turned on at maximum brightness. We therefore conducted a series of experiments to determine if this temperature change could be minimized by adjusting the duty cycle of the μLEDs. We achieved acceptable brightness through these adjustments with less than 1°C increase in temperature (fig. S4).

Next, to continuously evaluate the integrity of the insulation materials for the μLEDs and impose preventive measures to shut down the iEEG-microdisplay upon insulation material degradation or failure, the impedance of all the electrically conducting elements (metal traces, Ohmic contacts, and the GaN) of the μLEDs in relation to the brain tissue was monitored every 10 seconds throughout the entire 3.7-hour duration of pig brain recording. This test revealed no detectable changes in the impedance, indicating that no electrical leakage paths developed and the conformal attachment was preserved for the duration of the experiment (Fig. 1D and fig. S5). To test the validity of our impedance monitoring setup and to ensure it properly represents electrical leakage paths, scratches were purposedly made on the surface of the μLED array. In this setting, a clear drop in impedance was observed whenever there was mechanical or electrical damage to the device (Fig. 1D), indicating that our impedance monitoring setup was reliable in detecting the presence of electrical leakage paths in the iEEG-microdisplay. The extended soak test of the iEEG-microdisplay in saline solution over 7 days revealed that the device's impedance remained stable throughout a week (Fig. S6), further emphasizing the device's durability in a moist environment.

The iEEG-microdisplay allows anatomical mapping of functional M1/S1 boundaries on the surface of the brain

The precise localization of the central sulcus, the anatomical boundary between primary motor (M1) and somatosensory (S1) cortices, is crucial in tumor and epileptogenic tissue resections in these brain regions. This boundary is identified at the point where somatosensory evoked potentials (SSEPs) in response to peripheral nerve stimulation exhibit opposite polarity in their potentials commonly recognized by either a negative phase (P20) and the positive phase (N20)(33, 34). Commonly, the presence of pathological tissue can shift this functional boundary from its anatomical organization(7, 35). To test whether the iEEG-microdisplay can directly project the M1/S1 boundary from the surface of the brain based on physiological signatures, we applied the 32mm × 32mm iEEG-microdisplay across the mid-line of the pigs' brain covering both the left and right primary motor cortex (M1) and primary somatosensory cortex (S1). To evoke SSEPs, we stimulated the peripheral nerves with subdermal twisted pair needles placed in the pig's left and right forelimbs (Fig 2A, 10mA, 1ms biphasic pules). Small stimulus artifact prior to high amplitude SSEPs were observed within 10 to 50ms post-stimulation, followed by SSEPs that exhibited phase reversal indicated by the red arrow-heads of Fig. 2B (36). The iEEG-microdisplay

revealed a cortical functional boundary (FB) between the primary somatomotor (M1) cortex and primary somatosensory (S1) cortex depicted with a line of illuminated μLEDs in the hemisphere contralateral to stimulation (Fig. 2, C to H, fig. S7). The displayed FB was in accordance the offline analysis of raw potential waveforms done with the P20-N20 potential mapping (Figs. 2D and G, fig. S8) and correlation coefficient mapping (Fig. 2E and H). When using a dual color iEEG-microdisplay, FBs were represented by a change of color from green to red (Fig. 2, I and J).

The iEEG-microdisplay allows to identify functional cortical columns from the surface of the brain

To demonstrate the advanced mapping and display capabilities of the iEEG-microdisplay, we conducted a localized sensory mapping on an anesthetized pig by administering electrical or air-puff sensory stimuli to different areas of the pig's face and limbs thereby evoking high gamma responses on the brain's surface (Fig. 3A). The high gamma activity (HGA) was mapped for each of n=50 trials, and the trial averaged HGA mapping was updated and displayed – every 1 s – on the brain's surface whenever a new stimulus was administered. Skin electrical stimulation (2mA, 1ms, biphasic, bipolar) of left and right forelimbs, cheeks, and tongue was administered to reveal uniquely distinguishable cortical regions and simultaneously observe the anatomical features of the brain tissue underlying the iEEG-microdisplay (Fig. 3, B to G, fig. S9). We hypothesized that local air-puff stimulation on the surface of the skin delivered through a microcapillary tube can lead to focal responses when compared to gross-sum activation of nerve fibers by electrical stimulation in the vicinity of the stimulating needle probes(37). Indeed, with nerve electrical stimulation, HGA responses were less localized (Fig. 3D) compared to responses to air-puff stimulation of the tongue tip (Fig. 3G). These results were corroborated by responses of electrical or air-puff stimulations of the pig's snout depicted in waveforms (Fig. 3, H and I and fig. S9) and the spatial mapping of the HGA (Fig. 3, J to L). The potential evoked by air-puff stimulation of two different snout positions (Fig. 3I) showed a single peak near 35ms whereas the electrically stimulated snout showed multiple peaks from 10 to 90ms, the latter presumably due to the volumetric stimulation of multiple different types of sensory and motor neurons with varying latencies(38). The iEEG-microdisplay depicted relatively broader spatial maps of HGA responses evoked by electrical stimulation of the snout (Fig. 3J) and tightly localized HGA by air-puff stimulation of two different spots (Fig. 3, K and L) within the electrically responsive region of Fig. 3J. These HGA mappings displayed on the brain surface were in agreement with the offline analysis on measured raw potential waveforms from PtNRGrids μECoG (Fig. 3. M and N) that shows spatial mapping of HGA together with trial-averaged raw waveforms (n=50 trials).

Next, we applied the 5mm × 5mm high-resolution iEEG-microdisplay to the barrel cortex of the rat to isolate the location and boundaries of sub-millimeter-scale cortical columns (Fig. 3O). The rat barrel cortex is a well-studied system where specific sensory cortical columns have a one-to-one mapping with individual whiskers(39). While air-puffs stimulated the individual whiskers, we recorded and displayed the spatial map of trial averaged (n=55 trials) HGA. We observed that a small group of μLEDs were selectively lit up in clearly distinct positions at sub-millimeter scale indicating individual positions of cortical columns

that correspond to each whisker (Fig. 3P). When all whiskers in the field-of-blow were air-puff stimulated, a larger group of μLEDs were lit up with a diameter near 3 mm, indicative of the extent of multiple whisker barrel cortices (Fig. 3P). When compared with the spatial mapping by offline analysis of recorded waveforms (Fig. 3Q), the spatial mapping of raw waveforms and HGA (n=55 trials) (Fig. 3, R and S) were in agreement with the HGA displayed with iEEG-microdisplay.

The iEEG-microdisplay allows brain surface mapping of neuronal activity in response to direct electrical stimulation

Direct electrical stimulation of the brain and observation of behavioral responses and after-discharges inform the location and boundaries of diseased tissue and is typically carried out with a handheld bipolar cortical stimulator (Ojemann probe)(40). This procedure is generally performed on the exposed brain without any grid on the surface. Our iEEG-microdisplay was designed with large-diameter through-hole arrays (0.5 mm diameter with 1 mm pitch) throughout the grid (fig. S10). These perforations permitted the delivery of stimulation with the Ojemann probe to any position of the pig brain together with the simultaneous display of the extent of the resultant electrical potential and the brain's response (Fig. 4, A to C). We administered charge-balanced biphasic pulses of 3 mA and 50 Hz with varying durations between 0.1 s to 1.9 s and recorded and displayed the root mean square (RMS) of the voltage brain wave responses within the frequency range of 10-59 Hz. The refresh rate of the iEEG-microdisplay was 40 Hz as we processed 25ms data packets from 1024 channels and displayed the RMS map every 25ms. Fig. 4A shows the iEEG microdisplay and the Ojemann proble placed on the pig’s brain prior to stimulation. During brain stimulation, a large electrical potential was created causing many μLEDs in the array to light up around each side of bipolar probe (Fig. 4B). After the stimulation, we observed a post-stimulus pattern around the bipolar probe near 200 ms (Fig. 4C). The RMS potential map observed in real-time on the brain surface was in good agreement with the offline analysis of measured raw potential waveforms form PtNRGrids μECoG where the spatial map of raw waveforms was overlaid with the RMS potential map (Fig. 4, D and E).

In addition to the stimulation of the brain surface with an Ojemann probe, depth electrode stimulation was also used to map corticocortical structures. To this end, we inserted a stereoelectroencephalography (sEEG) probe (0.8 mm diameter, contact spacing of 6 mm) into the depth of the brain (Fig. 4F) next to the iEEG-microdisplay (see the position marked in Fig. 4, F and G). We then applied bipolar, biphasic stimulation pulses (4 mA, 0.5 ms, single pulse) between adjacent contacts at depths of 9 mm and 3 mm, respectively. Under a single pulse stimulation, a population of pink LEDs lit up around the sEEG stimulation site indicating a clear spatial display of post-stimulus potentials on the brain surface (Fig. 4G). Here, a dual-color iEEG-microdisplay with 2048 μLEDs displayed a statically lit HGA corresponding to the forelimb in blue and the real-time evolution of the RMS potentials in pink (Fig. 4F). The spatial pattern of the responses observed on the iEEG-microdisplay was in good agreement with the offline analysis which overlaid the post-stimulus RMS potential map (35-60 ms, 10-59 Hz) together with the spatial map of waveforms including the stimulation pulse (−100 to 300 ms) (Fig. 4H). These results illustrate that the iEEG-

microdisplay provided real-time feedback of stimulation responses directly from the surface of the brain (Movies S1 and S2).

The iEEG-microdisplay allows to monitor pathological wave dynamics

A final important feature of the iEEG-microdisplay is its ability to facilitate high-resolution mapping of pathological brain activity. For example, the precise intraoperative neuromonitoring to detect the onset zones of seizures and patterns of their spread is essential for successful treatment.(41) To demonstrate pathological brain activity such as epileptiform activity could be displayed using the iEEG-microdisplay, we placed the display over the anesthetized pig's brain and artificially induced epileptic seizures by applying neurotoxins on the brain underlying the display (Fig. 5A). This procedure included the administration of three types of neurotoxins, with each toxin administered to separate animals: (1) Bicuculline (BIC) crystals that were topically applied on the brain surface, (2) the sub-cortical injection of 4-Aminopyrodine (4-AP) or Penicillin-G (Pen-G). All three types of neurotoxins induced epileptiform activities whereas BIC induced the most prominent responses showing large amplitude epileptiform activities (approximately 0.5mV peak-to-peak) (Fig. 5B). After the initial observation of the epileptiform activity (which occurred 3 minutes after the application of BIC) the frequency of epileptiform activities rapidly increased over each subsequent minute (Fig. 5C). Six minutes after the BIC application, spatial mapping of large voltage deflections (10-59 Hz) through RMS detections revealed clear and repetitive voltage deflections (likely correlated to epileptiform activity) within a few millimeters around the BIC application point during the case.

We conducted further investigation into the origin and spatiotemporal dynamics of epileptiform activity using streamlines to indicate the propagating direction of brain waves(21). The spatial mapping of epileptiform discharge events was analyzed using the spatial mapping of potentials in band-pass filtered data (10-59 Hz) and streamlines derived from phase gradient analysis(42). The epileptiform activity (Fig. 5D) revealed an epileptiform discharge wave originating near the BIC application site which then propagated outward as represented by the white streamlines (Fig. 5D). Conversely, the second epileptiform event occurred about 500ms after the first and showed the epileptiform discharge wave propagating in the reverse direction, back toward the origin of the first epileptiform discharge. To ascertain whether the observed epileptiform waves were pathological interictal discharges (IID), we utilized offline automatic detection algorithms commonly employed for identifying IIDs(43) combined with visual confirmation by an experienced epileptologist (SSC). We found overlap between the detected IIDs and the spatially located RMS detections near the site of the BIC application (Fig. 5, C to E). This spatial mapping of the spike rate for the detected voltage deflections possibly correlating to IIDs (Fig. 5E) correlated to the displayed RMS-measured voltage changes on the surface of the pig's brain using the iEEG-microdisplay (Fig. 5F). The images were captured under blue-light blocking glass (>550 nm long pass filter, fig. S2) to enhance the distinction between the green and red colors displayed by the dual-color μLED arrays. While displaying the M1/S1 boundary as a static green line, the large voltage deflections possibly correlating with IIDs were shown in real-time in red. Using this iEEG-microdisplay, a pathological wave likely correlating to an IID was observed originating near the BIC application site

which propagated to the left side. A consecutive event then showed these voltage deflections propagating back in the reverse direction (Fig. 5F, Movie S3). These observations are consistent with the findings from our offline analysis (Fig. 5, D and E). The voltage waves likely correlating with IIDs propagated back and forth repeatedly from the BIC application site throughout the entire one-hour experiment duration. Moreover, when another BIC dose was administered on the rightmost side of the grid, a large voltage wave originating and propagating from the new application site was observed (fig. S11). Similar propagating behavior of pathological waves was observed when 4-AP (Fig. 5G) or Pen-G (fig. S12) were injected sub-cortically.

For future clinical application of the iEEG-microdisplay it would be essential to detect and display pathological activities which would be co-registered to functional regions in the cortex. To this end, the cortical regions responding to electrical stimulation of the forelimb were mapped and displayed as a static green spot while real-time evolution of the pathological activity was shown dynamically as it occurred in red (Fig. 5G). The large repetitive voltage waveforms which are likely IIDs originated near the 4-AP injection site and propagated and spread away from that site. This shows that the iEEG-microdisplay technology could be used to communicate multiple types of information, display functional boundaries in green color, and show high-resolution real-time videos of pathological waves with red.

Lastly, we evaluated the iEEG-microdisplay's capacity to detect and display fine scale pathological activity at a high-resolution. The iEEG-microdisplay was positioned on the barrel cortex of a rat after which epileptiform activity was induced by topical application of BIC next to cortical surface next to the iEEG-microdisplay. Similar to the case of the pig, the first voltage event which is a putative IID occurred 3 minutes after administering BIC to the barrel cortex of the rat. The frequency of these voltage deflections increased to 4 spikes per minute at the 5-minute mark (Fig. 5H), with a substantial peak-to-peak amplitude of 3 mV. After 20 minutes had elapsed since the first BIC dose, the voltage deflections amplitude decreased to 1 mV peak-to-peak, and the same spiking rate of 4 spikes per minute continued from the 5-minute mark. We also applied propagating wave analysis to the observed events by overlaying the potential map (filtered in the frequency range of 10-59 Hz) and streamlines representing the instantaneous propagating characteristics of pathological brain waves analyzed by the phase gradient (Fig. 5I). These putative IIDs on the rat brain surface were visible in real-time, as shown by the series of images at each time point (Fig. 5J) and supplementary video (Movie S4). We repeatedly observed the IIDs originating near the BIC application site and propagating and spreading out to the left side. These findings demonstrate that the iEEG-microdisplay allows to display submillimeter-scale pathological wave dynamics in real-time.

DISCUSSION

We developed an iEEG-microdisplay that allows to display the dynamics of brain cortical activity in real-time.

The iEEG-microdisplay is composed of flexible 1024 or 2048 μLED arrays, combined with 1024 channel PtNRGrids and associated hardware and software for real-time display. This design enabled mapping of normal and pathological activities in sub-mm resolution over the extent of centimeter range. With its high spatial and temporal resolution of neural activity and real-time visual feedback, the iEEG-microdisplay offers a potential improvement over current intraoperative brain mapping practices. The flexible μLED arrays built on thin, semi-transparent, and conformal polyimide substrates can be reconfigured in pitch to achieve wide cortical coverage. Multiple colors can be displayed to indicate different types of cortical activity. The iEEG-microdisplay is scalable and provides real-time feedback on neural activities in response to external stimulation. In the future, the iEEG-microdisplay can be used to visualize healthy and diseased brain regions and their boundaries directly from the surgical field (Fig. S14).

However, our study has limitations. The close proximity of the μLED system and μECoG grid led to interference, causing high-frequency noise to be added to the ECoG signals when the μLED system was powered on. This interference resulted from the microdisplay being driven by high-frequency 5V pulses, even when the LEDs were not emitting light. The noise appeared as multiple peaks in the power spectral density plots, typically starting at 98.63 Hz and its harmonics (see fig. S13). Despite these noise issues, we were still able to effectively extract meaningful neurophysiological signals, displaying important cortical functional boundaries and propagation of IIDs. To further reduce the noise, we plan to implement customized hardware to drive the μLEDs at higher pulse rates in future iterations of the device. This adjustment would result in the noise peaks currently at 98.63 Hz and 197.37 Hz being shifted to frequencies above 200 Hz. By ensuring that all noise peaks surpass the high gamma frequency bands, we can implement a low pass filter with a cutoff below 200 Hz to effectively isolate brain wave signals with minimal noise. Additionally, we envision to implement in future iterations ground traces between LED line traces can be used to further attenuate the resulting electromagnetic noise induced by the traces used to switch the LEDs.

To translate this technology to human application, the system must be able to perform continuous and high sensitivity measurements for the detection of leakage currents preferably on each metal line. This approach could replace the intermittent impedance measurements performed every 10 s. Although the PtNRGrid passed the biocompatibility, sterility, and packaging requirements for clinical translation, these tests must be performed on the completely assembled iEEG-microdisplay for use in humans. For full color display, lamination of three red, green, and blue GaN μLEDs will be required as opposed to the color conversion scheme presented here for binary display of normal and pathological brain activity. With the increase of the spatial resolution toward high-definition display, the transparency of the iEEG-microdisplay can be compromised. However, with the high-frame display, it is possible to project the anatomical features as a static image on the iEEG-microdisplay and simultaneously display normal and pathological activity in real-time.

The future dissemination of the iEEG-microdisplay should also account for its cost. We estimate that the cost of goods for a single PtNRGrid to be approximately $500 –using the 7” × 7” glass plate substrate – and for a single GaN μLED array to be approximately

$600 on the 6” GaN-on-QST substrate and using equipment in our research facilities. Accounting for labor cost, the current overall cost of the iEEG-microdisplay will be higher than the cost of clinical ECoG grid technology, yet reasonable. The whole GaN μLED array transfer developed here is low cost when compared to flip-chip array integration of individual μLEDs. It is also important to note that the concept of the iEEG-microdisplay encompasses the combination of ECoG technology and of LED technology irrespective of the materials used provided that they offer comparable or better performance than what is presented here. At the large dissemination scale, we envision that the cost of iEEG-microdisplay to be comparable to or lower than that of a cell phone screen, which is currently a few tens of dollars. An overall end-to-end solution with software display and analysis will likely have a cost that is comparable to that of a cell phone. Lastly, it would be desirable to excise tissue while the iEEG-microdisplay is placed on the brain’s surface without interfering with its function. We envision that creating a foldable portion within the iEEG-microdisplay can create a window-in-grid for operation. Additionally, most tissue excisions in the brain are performed with ultrasonic vibration and suction and as such, the potential integration of ultrasound micro-transducers next to the PtNRGrid may provide the capability of performing micro-excisions for diseased tissue without severely compromising its conformity. With light directed toward the cortical surface, the iEEG-microdisplay could be used for high-resolution optogenetic stimulation.

In conclusion, the iEEG-microdisplay has the potential to improve brain activity mapping for basic neuroscience as well as neurosurgical practices.

MATERIALS AND METHODS

Study Design:

Objectives of the study were to design, fabricate, and validate the effectiveness and utility of the iEEG microdisplay for real-time visualization of cortical activity. The methodology involved fabricating the iEEG-microdisplay which included the fabrication of flexible μLED arrays and of μECoG electrode grids and their integration, as well as the testing its effectiveness for real-time brain activity mapping in both pig and rat. Key metrics evaluated included device stability, precision in activity mapping, and safety of operation validated by postmortem histology. The ultimate goal was to validate the iEEG microdisplay as an effective instrument for offering high-resolution, real-time visualization of brain activity that holds promise for improving neurosurgical outcomes in future studies. We used proof of concept experiments in rats and pigs to test the capacity of the iEEG-microdisplay to monitor brain activity and functional borders in form of spatially registered light patterns on the brain surface. We successfully recorded surface μECoG signals and displayed activity with LEDs in real time from six rats and six pigs. Given the exploratory and qualitative focus of our study on the iEEG microdisplay, sample size was not predetermined. The data collected from animals using early prototypes of the iEEG-microdisplay were excluded from the study. The number of trials in a specific animal model recording was determined when functional cortical mapping reached its saturation point. Each experimental paradigm included controls for acquiring a baseline recording prior to or throughout the given recording period. Data acquisition was not blinded, and we did not include a randomization

of subject selection in this study. No statistical tests were used in this study, as our aim was to qualitatively assess the iEEG microdisplay's functionality and its application in real-time cortical activity visualization.

All procedures for the rat and pig experiment were approved by the UCSD Institutional Animal Care and Use Committee under protocol S16020 and S19030, respectively.

Supplementary Material

Refer to Web version on PubMed Central for supplementary material.

Acknowledgements

The authors are grateful for the technical support from the nano3 cleanroom facilities at UC San Diego's Qualcomm Institute where the fabrication of the iEEG-microdisplay was conducted. The authors are thankful to Qromis, Inc., for providing the GaN LED substrates. The authors are also grateful for the staff support at the Center of the Future of Surgery at UC San Diego where the pig animal surgeries and experiments were conducted. This work was performed in part at the San Diego Nanotechnology Infrastructure (SDNI) of UC San Diego, a member of the National Nanotechnology Coordinated Infrastructure, which is supported by the National Science Foundation (Grant ECCS1542148).

Funding

This work was supported by the National Institutes of Health primarily through Award No. NIBIB DP2-EB029757 (to S.A.D.) and in part by the BRAIN® Initiative NIH grants R01NS123655 (to S.A.D.), K99NS119291 (to K.J.T.), UG3NS123723 (to S.A.D.) and 5R01NS109553 (to E.H.). Any opinions, findings, and conclusions or recommendations expressed in this material are those of the author(s) and do not necessarily reflect the views of the funding agencies.

References and Notes

1. Karschnia P, Vogelbaum MA, van den Bent M, Cahill DP, Bello L, Narita Y, Berger MS, Weller M, Tonn J-C, Evidence-based recommendations on categories for extent of resection in diffuse glioma. European Journal of Cancer 149, 23–33 (2021). [PubMed: 33819718]
2. Cahill DP, Extent of resection of glioblastoma: A critical evaluation in the molecular era. Neurosurgery Clinics 32, 23–29 (2021). [PubMed: 33223023]
3. Krishna S, Choudhury A, Keough MB, Seo K, Ni L, Kakaizada S, Lee A, Aabedi A, Popova G, Lipkin B, Glioblastoma remodelling of human neural circuits decreases survival. Nature, 1–9 (2023).
4. Englot DJ, Han SJ, Berger MS, Barbaro NM, Chang EF, Extent of surgical resection predicts seizure freedom in low-grade temporal lobe brain tumors. Neurosurgery 70, 921–928 (2012). [PubMed: 21997540]
5. Mohan M, Keller S, Nicolson A, Biswas S, Smith D, Osman Farah J, Eldridge P, Wieshmann U, The long-term outcomes of epilepsy surgery. PloS one 13, e0196274 (2018). [PubMed: 29768433]
6. Shah P, Bernabei JM, Kini LG, Ashourvan A, Boccanfuso J, Archer R, Oechsel K, Das SR, Stein JM, Lucas TH, High interictal connectivity within the resection zone is associated with favorable post-surgical outcomes in focal epilepsy patients. NeuroImage: Clinical 23, 101908 (2019). [PubMed: 31491812]
7. Duffau H, Sichez JP, Lehéricy S, Intraoperative unmasking of brain redundant motor sites during resection of a precentral angioma: evidence using direct cortical stimulation. Annals of neurology 47, 132–135 (2000). [PubMed: 10632114]
8. Duffau H, Capelle L, Sichez J-P, Faillot T, Abdennour L, Law Koune J-D, Dadoun S, Bitar A, Arthuis F, Van Effenterre R, Intra-operative direct electrical stimulations of the central nervous system: the Salpetriere experience with 60 patients. Acta neurochirurgica 141, 1157–1167 (1999). [PubMed: 10592115]

9. Skirboll SS, Ojemann GA, Berger MS, Lettich E, Winn HR, Functional cortex and subcortical white matter located within gliomas. Neurosurgery 38, 678–684; discussion 684 (1996). [PubMed: 8692384]
10. Yang T, Hakimian S, Schwartz TH, Intraoperative ElectroCorticoGraphy (ECog): indications, techniques, and utility in epilepsy surgery. Epileptic Disorders 16, 271–279 (2014). [PubMed: 25204010]
11. Duffau H, Lopes M, Arthuis F, Bitar A, Sichez J, Van Effenterre R, Capelle L, Contribution of intraoperative electrical stimulations in surgery of low grade gliomas: a comparative study between two series without (1985–96) and with (1996–2003) functional mapping in the same institution. Journal of Neurology, Neurosurgery & Psychiatry 76, 845–851 (2005). [PubMed: 15897509]
12. Borchers S, Himmelbach M, Logothetis N, Karnath H-O, Direct electrical stimulation of human cortex—the gold standard for mapping brain functions? Nature Reviews Neuroscience 13, 63–70 (2012).
13. Swift J, Coon W, Guger C, Brunner P, Bunch M, Lynch T, Frawley B, Ritaccio A, Schalk G, Passive functional mapping of receptive language areas using electrocorticographic signals. Clinical Neurophysiology 129, 2517–2524 (2018). [PubMed: 30342252]
14. Aabedi AA, Lipkin B, Kaur J, Kakaizada S, Valdivia C, Reihl S, Young JS, Lee AT, Krishna S, Berger MS, Functional alterations in cortical processing of speech in glioma-infiltrated cortex. Proceedings of the National Academy of Sciences 118, e2108959118 (2021).
15. Venkatesh HS, Morishita W, Geraghty AC, Silverbush D, Gillespie SM, Arzt M, Tam LT, Espenel C, Ponnuswami A, Ni L, Electrical and synaptic integration of glioma into neural circuits. Nature 573, 539–545 (2019). [PubMed: 31534222]
16. Haglund MM, Berger MS, Shamseldin M, Lettich E, Ojemann GA, Cortical localization of temporal lobe language sites in patients with gliomas. Neurosurgery 34, 567–576 (1994). [PubMed: 7516498]
17. Duffau H, Capelle L, Sichez J-P, Faillot T, Abdennour L, Koune J-DL, Dadoun S, Bitar A, Arthuis F, Van Effenterre R, Intra-operative direct electrical stimulations of the central nervous system: the Salpetriere experience with 60 patients. Acta neurochirurgica 141, 1157–1167 (1999). [PubMed: 10592115]
18. Southwell DG, Hervey-Jumper SL, Perry DW, Berger MS, Intraoperative mapping during repeat awake craniotomy reveals the functional plasticity of adult cortex. Journal of neurosurgery 124, 1460–1469 (2016). [PubMed: 26544767]
19. Kaiju T, Inoue M, Hirata M, Suzuki T, High-density mapping of primate digit representations with a 1152-channel μECoG array. Journal of Neural Engineering 18, 036025 (2021).
20. Chiang C-H, Wang C, Barth K, Rahimpour S, Trumpis M, Duraivel S, Rachinskiy I, Dubey A, Wingel KE, Wong M, Flexible, high-resolution thin-film electrodes for human and animal neural research. Journal of neural engineering 18, 045009 (2021).
21. Tchoe Y, Bourhis AM, Cleary DR, Stedelin B, Lee J, Tonsfeldt KJ, Brown EC, Siler DA, Paulk AC, Yang JC, Human brain mapping with multithousand-channel PtNRGrids resolves spatiotemporal dynamics. Science translational medicine 14, eabj1441 (2022). [PubMed: 35044788]
22. DenBaars SP, Feezell D, Kelchner K, Pimputkar S, Pan C-C, Yen C-C, Tanaka S, Zhao Y, Pfaff N, Farrell R, Development of gallium-nitride-based light-emitting diodes (LEDs) and laser diodes for energy-efficient lighting and displays. Acta Materialia 61, 945–951 (2013).
23. Shin J, Kim H, Sundaram S, Jeong J, Park B-I, Chang CS, Choi J, Kim T, Saravanapavanantham M, Lu K, Vertical full-colour micro-LEDs via 2D materials-based layer transfer. Nature 614, 81–87 (2023). [PubMed: 36725999]
24. Wierer JJ Jr, Tansu N III-Nitride micro-LEDs for efficient emissive displays. Laser & Photonics Reviews 13, 1900141 (2019).
25. Rajalingham R, Sorenson M, Azadi R, Bohn S, DiCarlo JJ, Afraz A, Chronically implantable LED arrays for behavioral optogenetics in primates. Nature Methods 18, 1112–1116 (2021). [PubMed: 34462591]

26. Zhu N, Mondal S, Gao S, Achilefu S, Gruev V, Liang R, Engineering light-emitting diode surgical light for near-infrared fluorescence image-guided surgical systems. Journal of biomedical optics 19, 076018–076018 (2014). [PubMed: 25057962]
27. Tanaka A, Choi W, Chen R, Liu R, Mook WM, Jungjohann KL, Yu PK, Dayeh SA, Structural and electrical characterization of thick GaN layers on Si, GaN, and engineered substrates. Journal of Applied Physics 125, 082517 (2019).
28. Odnoblyudov V, Aktas O, Basceri C, in Electrochemical Society Meeting Abstracts prime2020. (The Electrochemical Society, Inc., 2020), pp. 1814–1814.
29. Hu Z, Yin Y, Ali MU, Peng W, Zhang S, Li D, Zou T, Li Y, Jiao S, Chen S.-j., Inkjet printed uniform quantum dots as color conversion layers for full-color OLED displays. Nanoscale 12, 2103–2110 (2020). [PubMed: 31913379]
30. Ganji M, Paulk AC, Yang JC, Vahidi NW, Lee SH, Liu R, Hossain L, Arneodo EM, Thunemann M, Shigyo M, Selective formation of porous Pt nanorods for highly electrochemically efficient neural electrode interfaces. Nano letters 19, 6244–6254 (2019). [PubMed: 31369283]
31. Seese TM, Harasaki H, Saidel GM, Davies CR, Characterization of tissue morphology, angiogenesis, and temperature in the adaptive response of muscle tissue to chronic heating. Laboratory investigation; a journal of technical methods and pathology 78, 1553–1562 (1998). [PubMed: 9881955]
32. Kim S, Tathireddy P, Normann RA, Solzbacher F, Thermal impact of an active 3-D microelectrode array implanted in the brain. IEEE Transactions on Neural Systems and Rehabilitation Engineering 15, 493–501 (2007). [PubMed: 18198706]
33. Romstöck J, Fahlbusch R, Ganslandt O, Nimsky C, Strauss C, Localisation of the sensorimotor cortex during surgery for brain tumours: feasibility and waveform patterns of somatosensory evoked potentials. Journal of Neurology, Neurosurgery & Psychiatry 72, 221–229 (2002). [PubMed: 11796773]
34. Cedzich C, Taniguchi M, Schäfer S, Schramm J, Somatosensory evoked potential phase reversal and direct motor cortex stimulation during surgery in and around the central region. Neurosurgery 38, 962–970 (1996). [PubMed: 8727822]
35. Haseeb A, Asano E, Juhász C, Shah A, Sood S, Chugani HT, Young patients with focal seizures may have the primary motor area for the hand in the postcentral gyrus. Epilepsy research 76, 131–139 (2007). [PubMed: 17723289]
36. Wood CC, Spencer DD, Allison T, McCarthy G, Williamson PD, Goff WR, Localization of human sensorimotor cortex during surgery by cortical surface recording of somatosensory evoked potentials. Journal of neurosurgery 68, 99–111 (1988). [PubMed: 3275756]
37. Civillico E, Contreras D, Comparison of responses to electrical stimulation and whisker deflection using two different voltage-sensitive dyes in mouse barrel cortex in vivo. The Journal of membrane biology 208, 171–182 (2005). [PubMed: 16645745]
38. Maier S, Goebel U, Krause S, Benk C, Schick MA, Buerkle H, Beyersdorf F, Kari FA, Wollborn J, Somatosensory and transcranial motor evoked potential monitoring in a porcine model for experimental procedures. Plos one 13, e0205410 (2018). [PubMed: 30296297]
39. Keller A, in The barrel cortex of rodents. (Springer, 1995), pp. 221–262.
40. Ojemann GA, Brain organization for language from the perspective of electrical stimulation mapping. Behavioral and Brain Sciences 6, 189–206 (1983).
41. So EL, Integration of EEG, MRI, and SPECT in localizing the seizure focus for epilepsy surgery. Epilepsia 41, S48–S54 (2000).
42. Rubino D, Robbins KA, Hatsopoulos NG, Propagating waves mediate information transfer in the motor cortex. Nature neuroscience 9, 1549–1557 (2006). [PubMed: 17115042]
43. Janca R, Jezdik P, Cmejla R, Tomasek M, Worrell GA, Stead M, Wagenaar J, Jefferys JG, Krsek P, Komarek V, Detection of interictal epileptiform discharges using signal envelope distribution modelling: application to epileptic and non-epileptic intracranial recordings. Brain topography 28, 172–183 (2015). [PubMed: 24970691]
44. Cheng C-Y, Mao M-H, Photo-stability and time-resolved photoluminescence study of colloidal CdSe/ZnS quantum dots passivated in Al2O3 using atomic layer deposition. Journal of Applied Physics 120, 083103 (2016).

45. Carrillo-Carrión C, Cárdenas S, Simonet BM, Valcárcel M, Quantum dots luminescence enhancement due to illumination with UV/Vis light. Chemical Communications, 5214–5226 (2009). [PubMed: 19707627]

46. Muller L, Piantoni G, Koller D, Cash SS, Halgren E, Sejnowski TJ, Rotating waves during human sleep spindles organize global patterns of activity that repeat precisely through the night. Elife 5, e17267 (2016). [PubMed: 27855061]

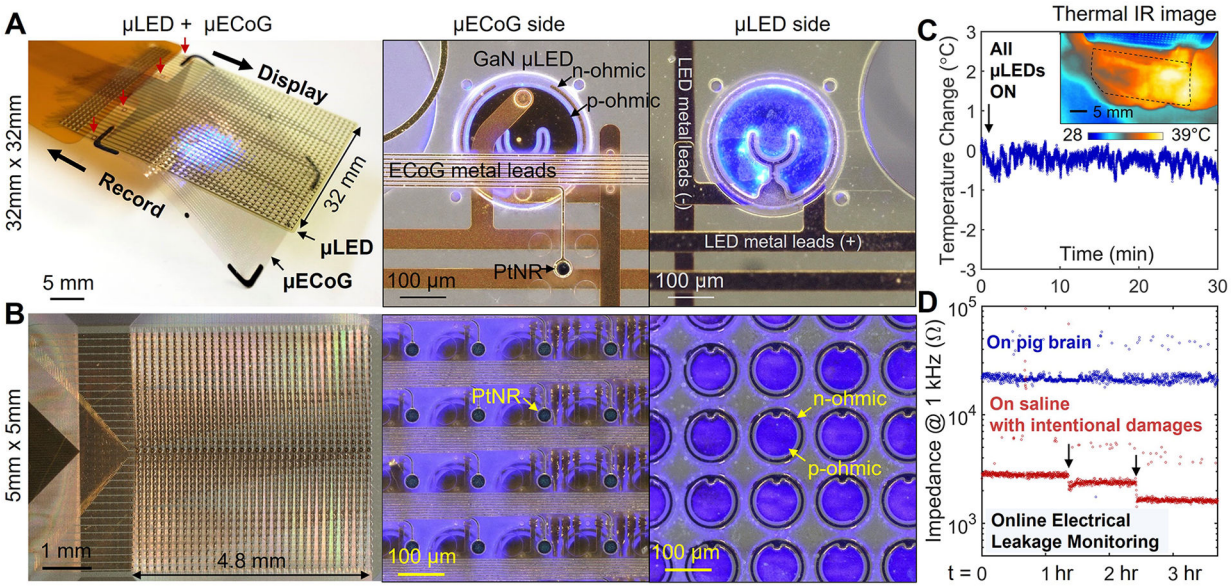

Figure 1. Fabrication process and safety evaluation of the iEEG-microdisplay.

A and B) Overview images of the Device structure and magnified OM images of 32mm x 32mm (A) and 5mm x 5mm (B) μLED+μECoG devices that integrated the flexible μLED arrays with 1024 pixels and PtNRGrids with 1024 channels. (C) Thermal safety evaluation of the iEEG-microdisplay by monitoring the cortical surface temperature of the pig brain (n=1) under 30 min continuous operation of all the LEDs. (D) Electrical safety evaluation of iEEG-microdisplay by monitoring the impedance of the device with respect to the brain tissues over 3.7 hours on the pig's brain (n=1).

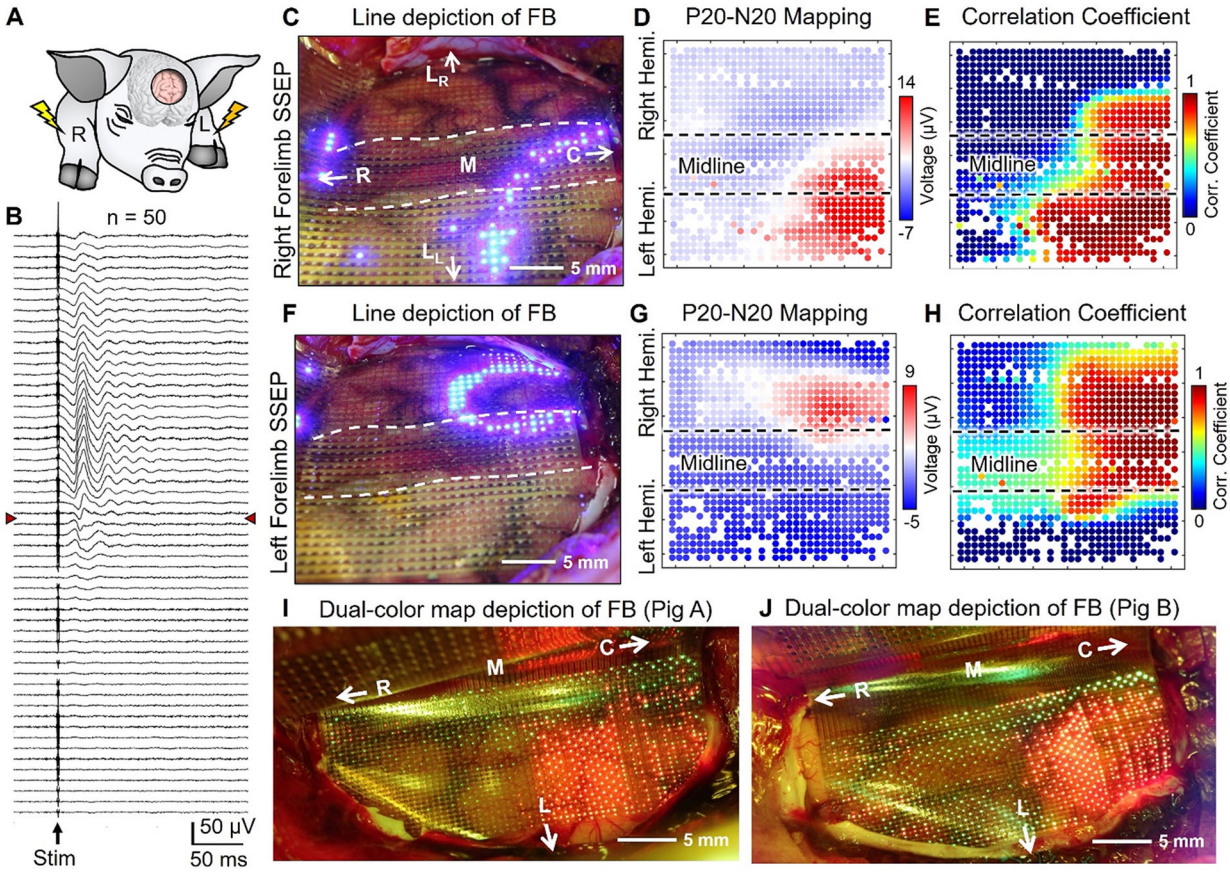

Figure 2. Real-time mapping and display of the primary somatomotor cortex (M1) and primary somatosensory cortex (S1) border on the cortical surface of pig brains.

(A) Schematics of the experiment depicting the electrical stimulation of the pig's left and right forelimbs (biphasic, bipolar pulse: 10mA, 1ms) while simultaneously recording SSEPs and displaying the M1/S1 boundary on the surface of the brain. (B) SSEP waveforms measured with dual-color iEEG microdisplay across an individual row of μECoG contacts across the M1/S1 boundary. The red arrowheads indicate the phase reversal boundary. (C) Representative images of an active single color (blue) 1024ch iEEG-microdisplay for the detection M1/S1 function boundary using right-forelimb stimulation. The corresponding offline analysis results showing (D) P20-N20 potential and (E) correlation coefficient mapping. (F) Representative images of active single color (blue) 1024ch iEEG-microdisplay for the detection M1/S1 function using left-forelimb stimulation and (G) corresponding offline analysis of P20-N20 potential and (H) correlation coefficient mapping. (I and J) Representative images of dual-color iEEG-microdisplay of motor/sensory boundary observed from; Pig A (image taken under 550 nm blue light blocking lens) and Pig B. (C)-(H): Representative results are presented from 1 out of 2 pigs with bilaterally placed single color μLEDs (Pig model #4). fig. S7 shows similar representative results from the other pig (Pig model #3). (I)-(J): Representative results are presented from 2 out of 2 pigs with unilaterally placed dual-color μLEDs.

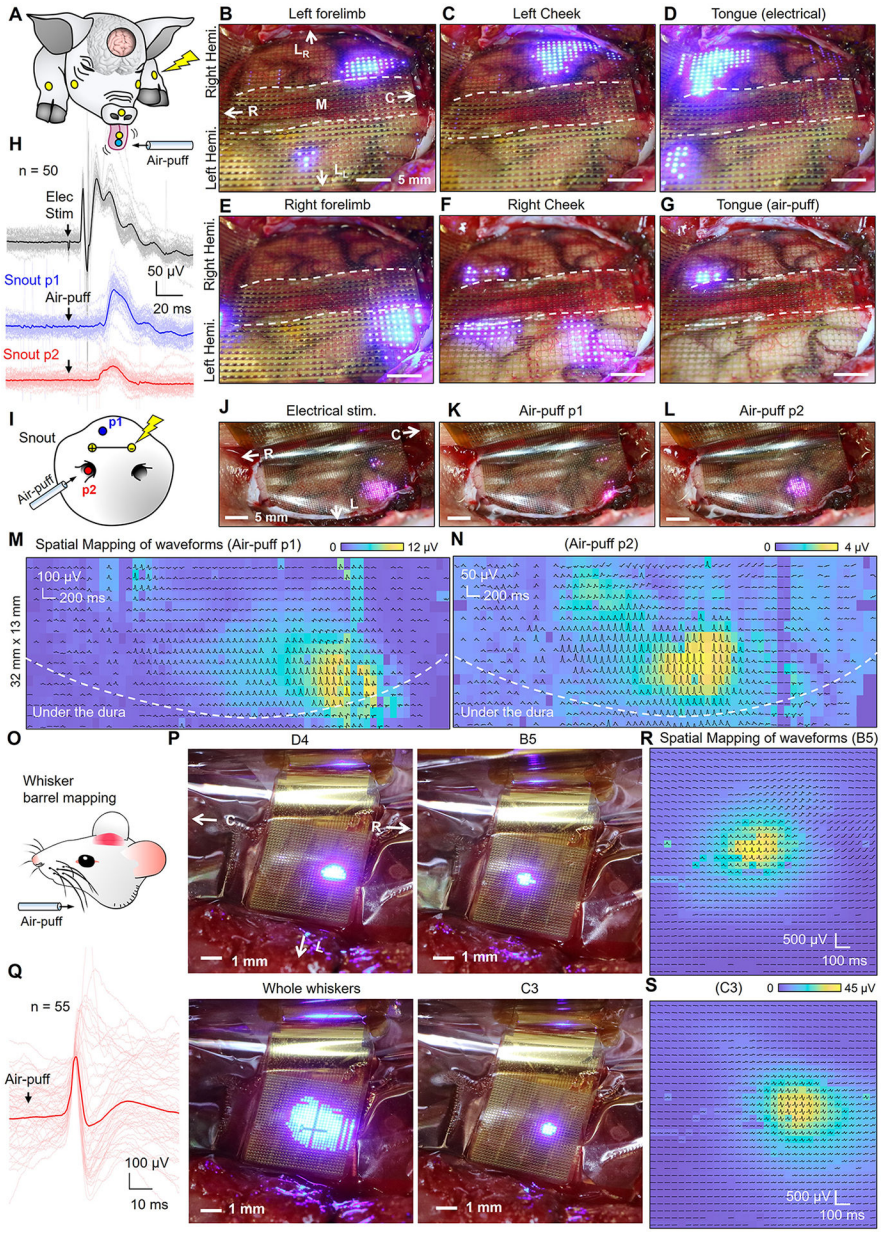

Figure 3. Sensory mapping and display on the cortical surface of pig and rat brain.

(A) Schematics showing the locations and type of sensory stimuli on different body parts of the pig. (B-G) High gamma activity (HGA) mapping of the electrical stimulation evoked responses (n=50 trials) of left forelimb (B), left cheek (C), tongue (D), right forelimb (E), and right cheek (F) . (G) HGA mapping evoked by air-puff stimulation of tongue tip from the same pig (H) Trial average SSEP waveforms (n=50 trials) overlaid with waveforms of individual trials under the electrical and air-puff stimulation of snout. (I) Schematics of electrical and air-puff stimulations of pig snout. HGA mapping evoked by (J-L) HGA mapping of electrical stimulation on the snout (J), and air-puff stimulation on the snout at positions p1 (K) and p2 (L). M-N) Corresponding spatial mapping of HGA and trial-averaged raw waveforms (n=50 trials) evoked by air-puff of snout at p1 (M) and p2 (N)

positions. (O) Schematics of air-puff stimulation of rat whiskers. (P) HGA mapping of individual cortical column position of B5, C3, and D4 barrel cortices (n=55 trials). Overall area of barrel cortices was displayed by the multiple whisker stimulation. (Q) Trial average SSEP waveforms (n=55 trials) overlaid with waveforms of individual trials under the air-puff stimulation of whisker. (R-S) Spatial mapping of HGA and trial averaged waveforms (n=55 trials) by the air-puff stimulation of B5 (R) and C3 (S) whiskers. (B)-(H): Representative results are presented from 1 out of 2 pigs with bilaterally placed single color μLEDs (Pig model #4); fig. S9A shows representative results from the other pig (Pig model #3). (J)-(N): Representative results are presented from 1 out of 2 pigs with a unilaterally placed dual-color μLEDs (Pig model #6); fig. S9B shows representative results from the other pig (Pig model #5). (P)-(S): Representative results are presented from 1 out of 3 rats (Rat model #4). fig. S9C and S9D shows representative results from Rat model #3 and #5, respectively.

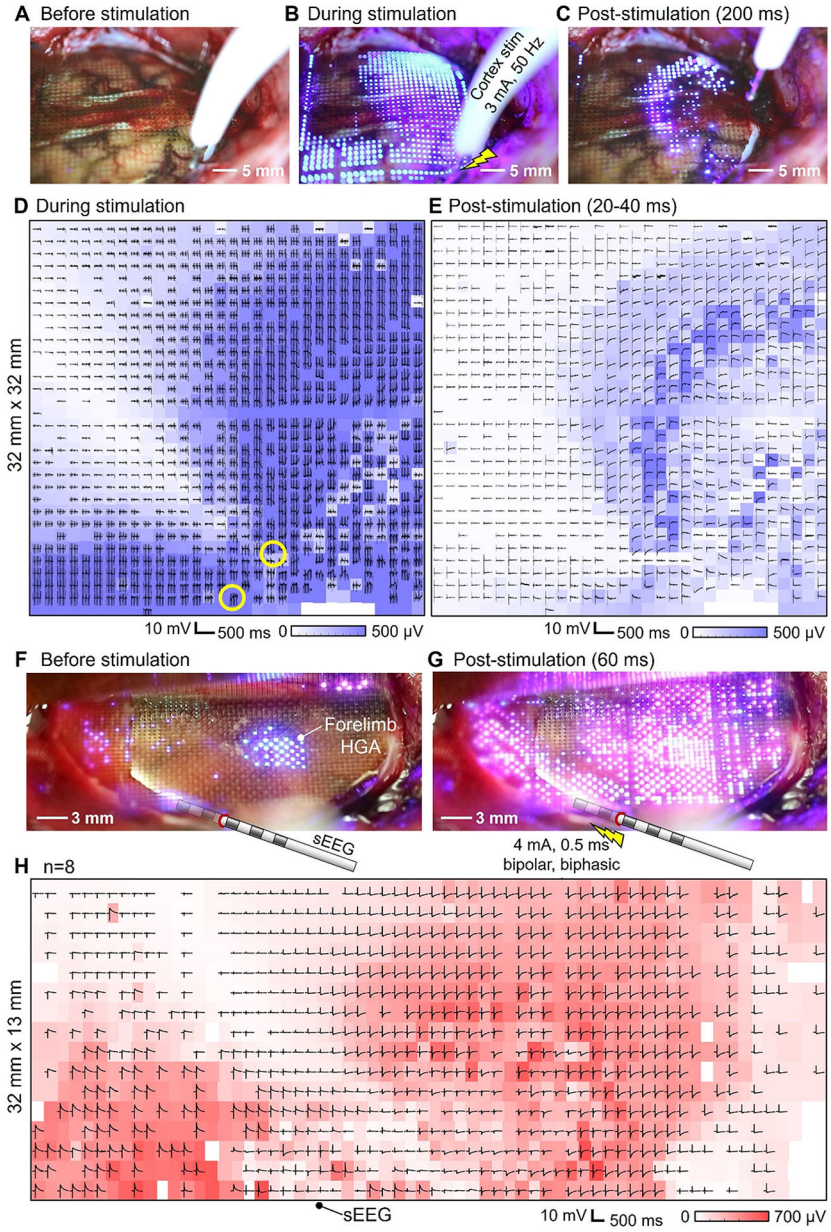

Figure 4. Display of electrical potentials in response to direct electrical stimulation on the cortical surface of pig brains

(A-C) Shown are representative images of the display of electrical activity before (B), during the electrical stimulation (3mA, 50 Hz)(A) and post stimulation (200 ms) (C) (D-E) Offline analysis of measured raw potential waveforms form PtNRGrids µECoG and RMS potential map (10-59 Hz) during the stimulation (−200 to 0 ms) (D) and after the stimulation (−10 to 200 ms) (E); the RMS potential map for (E) was obtained between 20-40 ms post-stimulus. (F-G) Shown are potential maps displayed on the cortical surface with ‘blue’ color (F) illustrating the HGA corresponding to forelimb and ‘pink’ color (G) illustrating the online potential map evoked by the 4 mA electrical stimulations by sEEG electrode between the pair of electrodes at the depth of 9mm and 3mm. (H) Trial-averaged (n=8 trials) waveform mapping (−100 to 300 ms) together with RMS potential map (35-60 ms, 10-59 Hz) after 4

mA single (left) and train (right) of pulses. (E) Trial averaged waveforms of sEEG electrical stimulation evoked responses from a single channel. (A)-(E): Representative results are presented from 1 out of 2 pigs with bilaterally placed and single color μLEDs (Pig model #3, see also Movie S1). Movie S5 shows electrical stimulation through iEEG microdisplay in the other pig (Pig model #4). (F)-(H): Representative results are presented from 1 out of 2 pigs with unilaterally placed dual-color μLEDs (Pig model #5, see also Movie S2). Movie S6 shows similar stimulation results from the other pig (Pig model #6).

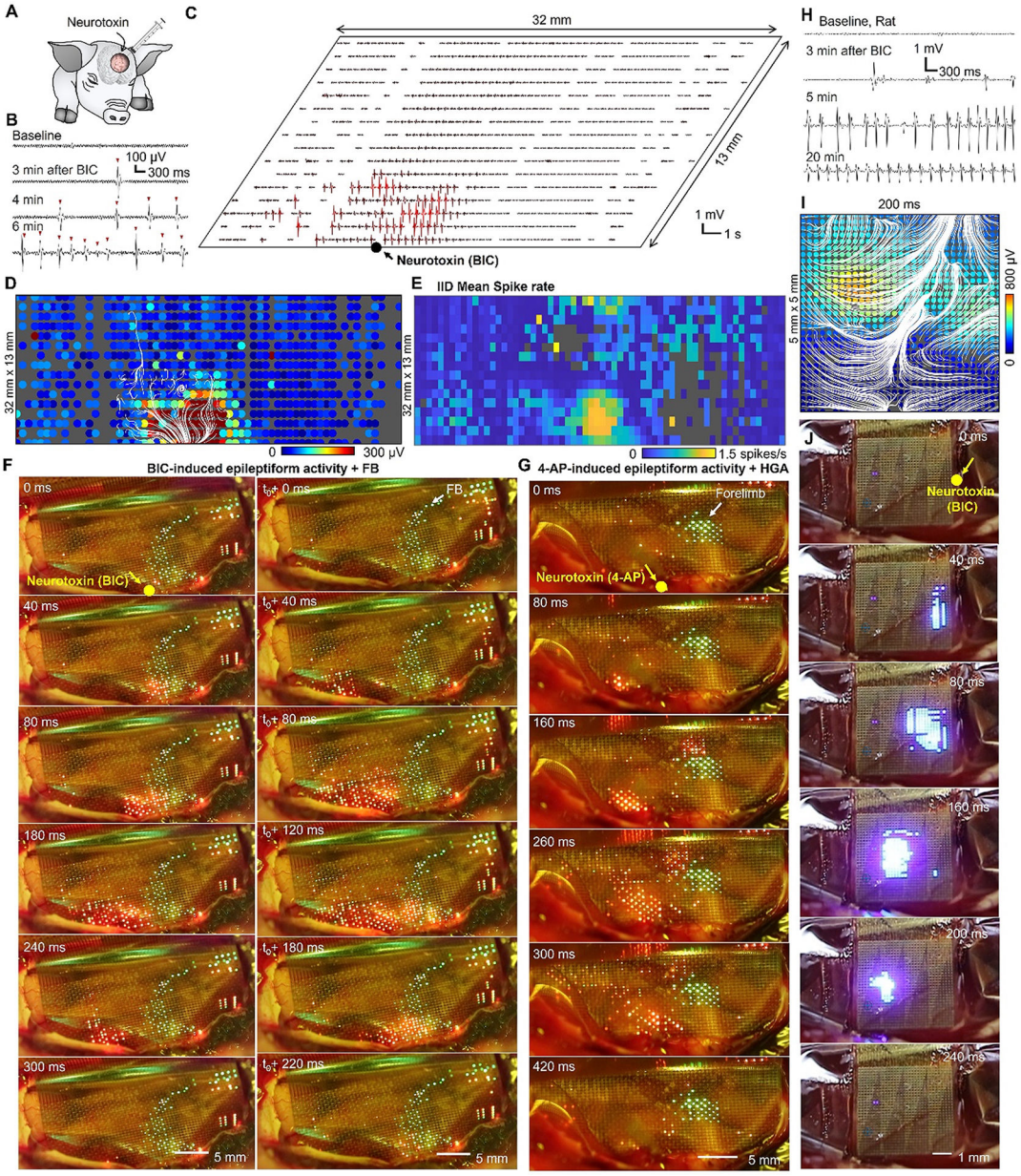

Figure 5. Mapping of epileptiform activity on the cortical surface of pig and rat brains.

(A) Schematics of experimental setup for evoking epileptiform activities on the pig brain by bicuculline (BIC) and 4-aminopyrodine (4-AP). (B) ECoG waveforms of baseline activity before and 3, 4, and 6 min after the application of BIC. (C) Spatial mapping of waveforms showing locally induced epileptiform activities around the topical application point of BIC crystals. (D-E) Spatial potential mapping of epileptiform spike overlaid with white streamlines depicting the propagating direction of the brain wave at 0 (D) and 540 ms (E). (F) Series of potential maps displayed on the cortical surface (under 550 nm blue blocking lens) with static ‘green’ color showing the motor/sensory functional boundary and dynamic ‘red’ color showing the online potential map of putative epileptiform activity under the BIC application on the cortex. BIC application point is marked as a yellow dot in the

first image. An outward propagating epileptiform wave from BIC application point was observed (left column), and after a short interval, t_0, an inward propagating epileptiform wave toward the BIC application point was observed (middle column). (G) 4-AP induced putative epileptiform activities on a different pig with green spot indicating the cortical area responsive to forelimb stimulation as identified with HGA mapping. (H) Waveforms of baseline activity and epileptiform activity induced on the rat brain by BIC over 3, 5, and 20 min. (I) Spatial mapping of putative IIDs together with the white streamlines showing the propagating direction of the putative epileptiform activities. (J) Displaying the putative epileptiform activities induced by BIC application. The original BIC application point is marked as a yellow dot. (A)-(E): Representative results are presented from pig with unilaterally placed dual-color μLEDs. (F)-(H): Representative results are presented from 1 out of 2 rats (Rat model #6). Movie S7 shows results from the other rat (Rat model #4).